



Electro-catalytic degradation mechanism of nitenpyram in synthetic wastewater using Ti-based SnO₂-Sb with rare earth-doped anode

Shanping Li*, Wenran Wang, Xueyuan Zeng, Xiangru Ma

School of Environmental Science and Engineering, Shandong University, Jinan 250100, China, Tel. +86 531 88362872; Fax: +86 531 88362872; email: lishanping@sdu.edu.cn

Received 26 November 2012; Accepted 2 February 2014

ABSTRACT

Nitenpyram (NIT), a kind of pyridine-based neonicotinoid insecticide, presents a high threat to water system. This work firstly examined the electro-catalytic (EC) degrading the NIT in synthetic wastewater by using the modified Ti/SnO₂-Sb anode, which was characterized by scanning electronic microscopy, X-ray energy dispersive spectroscopy, X-ray diffraction, and electrochemical measurement. The NIT removal and total organic carbon removal are monitored. The NIT EC treatment was found to obey the pseudo-first-order reaction kinetics within 60 min electrolysis and was controlled by the mass transport, the chemical reaction, and the oxygen evolution. Stable degradation intermediates were detected through electro-spray ionization quadrupole time-of-flight tandem mass spectrometry. Experiments indicated that several pyridine derivatives form during the EC process. Furthermore, the cleavage of pyridine ring could be demonstrated, which took place after the hydroxylation of the ring, leading to the complete mineralization of a NIT molecule. HO[•] and H₂O₂ played the dominant role in the EC degradation of NIT. The in situ-generating H₂O₂ was attributed to the reaction between dioxygen and α -amino radical.

Keywords: Electro-catalysis; Ti/SnO₂-Sb anode; Nitenpyram; Hydroxyl radicals; Wastewater treatment

1. Introduction

Neonicotinoids deriving from nictines are a kind of the principal alternatives for some synthetic pesticides such as organophosphate and carbamate [1,2], and have attracted the increasing attention in the agricultural sector worldwide. In the past three decades, they have been registered in more than 120 countries, accounted for 11–15% of the global insecticide market, and still kept a rapidly increasing application. Many literatures have reported to concern the

removal of neonicotinoid pollutants using advanced oxidation processes, which aimed at the complete mineralization. But the majority of them focus on the photolytic/photocatalytic oxidation of imidacloprid [3–7], acetamiprid [8–11], and thiacloprid [8–11].

Nitenpyram (NIT), a representative of the new generation neonicotinoid insecticides, was exploited in 1989 by Japanese Takeda Company and was made commercially available in 1991. Today, it is widely used in agriculture and horticulture to control sucking insects, such as thrips, whiteflies, hoppers, etc. and shows excellent activity on insects which are resistant to traditional insecticides [12,13]. Because of its

*Corresponding author.

widespread use and high water solubility (at temperature 293 K and pH 7, the solubility is 8.4×10^5 mg/L in water), NIT is presently increasing in the aqueous system [14]. However, the NIT molecule (its chemical structure is shown in Fig. 1) would not be rapidly degraded in natural water. At a temperature of 298 K and pH 7.0, NIT has a hydrolytic half-life of 415 days [15]. The accumulation of NIT in the environment can result in considerable environmental pollution, and ultimately bring a serious health-risk to humans. Moreover, NIT belongs to a kind of pyridine-based compounds, which are toxic to microorganisms. So, traditional biological treatment technology is generally difficult to remove NIT molecule in water or wastewater directly. Thus, it is exigent to investigate the degradation of NIT.

Recently, electro-catalytic (EC) advanced oxidation process has been proposed as an innovative alternative for the pre-treatment or treatment of wastewater containing recalcitrant toxic organic compounds like phenol [16], reactive brilliant red x-3b [17], 2-chlorophenol [18], and 2, 4-D [19], etc. The application of EC to environmental pollution abatement has been the topic of several reviews [20–24]. With the features of environmental compatibility and easy applicability to automation, it is significant to develop EC process as an efficient and economic method for the treatment of pyridine-based pollutants, especially for low-volume applications.

Electrode is the “heart” of electric catalytic system. In 1968, companies which were DeNora and Diamond Shamrock, successfully applied the DSA that was invented by Beer, to chlor-alkali production [25]. DSA anode quickly got the favor of people. After decades of development, DSA anode has been applied in many fields. Scholars at home and abroad, actively explored and chose a different surface-active component formula to prepare a series of new anode materials. Semiconductor oxide anode which has high electric catalytic activity, strong corrosion resistance and electrical conductivity, is one of the common electrode materials. Currently, the main compositions of semiconductor oxides were SnO_2 , PbO_2 , Sb_2O_5 , RuO_2 , IrO_2 ,

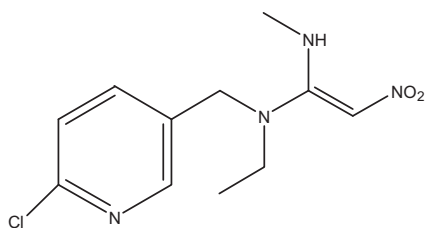


Fig. 1. The chemical structure of NIT.

Ta_2O_5 , or compounds which are made up of two or more [26–29]. The classification of the DSA anode and main application are listed in Table 1.

From Table 1, oxygen evolution potential of PbO_2 electrodes was not high, and electrochemical corrosion released the Pb^{2+} ion, which could cause secondary pollution of water. The prices of RuO_2 , IrO_2 , and so on with variable valence state of metal oxide anodes were expensive, and these anodes had advantages and disadvantages in terms of corrosion resistance and catalytic activity. Feng group in Harbin industrial university [30,31], studied several types of the electrodes' performance systematically. The research results showed that the Ti/SnSb electrodes for organic electric catalytic performance were superior to Pt, Ti/ PbO_2 , Ti, and Ti/ RuO_2 / IrO_2 anode materials, and showed the low resistivity and higher stability. So the Ti/ SnO_2 electrode was chosen [19].

In this work, NIT is the model pollutant. The main objective was to investigate the EC degradation of NIT in aqueous solution, particularly to do detailed analysis on its intermediates and products by means of electrospray ionization quadrupole time-of-flight tandem mass spectrometry (ESI-Q-TOF-MS). The degradation kinetic of NIT removal at different initial NIT concentrations was also studied. The working electrode was made by us and it was characterized by scanning electronic microscopy (SEM), X-ray energy dispersive spectroscopy (EDS), and X-ray diffraction (XRD). Accelerated life of the anode and cyclic voltammetry measurement were also obtained to evaluate the electrochemical prosperity of the anode.

2. Experimental details and analytical methods

2.1. Reagents

The original medicine of the NIT with a purity of 99% was purchased from Shandong Institute of Pesticide Research. All other chemicals and reagents used in this work were of analytical grade. Deionized water was used throughout the work.

2.2. Electrode preparation

Ti plates (3 cm length \times 5 cm width \times 0.07 cm thickness) were used as the base metals. The modified electrode with the mole ratio of Sn to Sb in 1:0.05 was synthesized by citrate sol-gel technique, following temperature-programmed thermal oxidation of the dipped inter-layer and surface-layer according to the procedures described in our previous literature [17]. On the base of the fact, introducing appropriate rare earth atoms into a SnO_2 -Sb anode could improve its

Table 1
Classification and application of DSA anodes

Classification	Main ingredients	Typical anode	Main purpose
Department of lead anode	PbO ₂	Ti/PbO ₂	Electrolytic refining, wastewater treatment
Department of ruthenium anode	RuO ₂	Ti/RuIrTi, Ti/RuO ₂	Chlor-alkali industry, electroplating, organic synthesis, cathodic protection, wastewater treatment of electrolytic refining, wastewater treatment
Department of iridium anode	IrO ₂	Ti/IrTa, Ti/IrO ₂	Organic synthesis, electroplating, wastewater treatment
Department of tin anode	SnO ₂	Ti/SnSb	Wastewater treatment

stability and EC degradation characteristics [17,32,33]. Pr (Pr/Sn mole ratio of 0.75%) and Dy (Dy/Sn mole ratio of 1.25%) were selected as promoters to be doped into the inter-layer and surface-layer, respectively. The annealing temperature was optimized at 903 K for 1 h.

2.3. EC treatment of NIT and analysis

In the electro-catalysis experiment, NIT synthetic wastewater with a 0.5 M Na₂SO₄ as the supporting electrolyte was used as the objective degradation solution. The aqueous solution of NIT (150 mL) was placed in an undivided cell with an electrode that was prepared by describing above as the anode material and a pure-Ti sheet as the cathode material, both of which had an electrolysis area of 5.4 cm² (3 × 1.8 cm). There was a space (3 cm) between these two electrode plates. The NIT degradation measurement was performed using an EC analyzer (CHI700B, Shanghai Chenhua Instrument Co., Ltd, China), cooperating with magnetic stir. Samples were taken out from the electrolysis wastewater for periodical analysis before and after degradation in the course of each run.

The concentration variation of NIT was measured by HPLC-DAD (UV-vis) by analyzing the absorption intensity change at its λ max of 270 nm [34]. An Agilent 1100 series chromatograph, coupling with a DAD detector was utilized. The absorption spectra of NIT were recorded with the UV-vis spectrophotometer within 180 min electrolysis time. The ESI-Q-TOF-MS was applied in the identification of intermediate products after 120 min NIT degradation. This method has been proved to be of high sensitiveness and accuracy in full scan of any practical compound in sample [35,36]. Prior to the analysis, the wastewater sample was extracted with ethanol. Extract liquid was directly injected into the ESI-Q-TOF-MS (Agilent, American), which was operated in positive ESI modeling with the spray voltage at 175 V. [M+H]⁺ was selected as the

precursor. In addition, total organic carbon (TOC) values were obtained by a TOC analyzer (SH-IMADIV 5000A). H₂O₂, a kind of active material generating in the NIT electrolysis was monitored by colorimetric method at the wavelength of 350 nm [37].

2.4. Electrode characterization

The morphologies of the surface layer of a freshly prepared electrode were done with a Japanese JEOL company model JSM-7600F microscope under magnification of 500X and 2000X. Fig. 2(a) and (b) present “cracked-clay” appearance typical of electrodes prepared by thermal oxidation.

The composition of elements coating on the electrode surface used a British Oxford INCA sight-X-ray EDS Electron spectrometer to analyze. The EDS spectra of double coating Pr and Dy-doped Ti/SnO₂-Sb electrode are shown in Fig. 3.

Considering the relative content of electrode coating metal elements, which influenced the electrode's EC properties, the content of Sn element was positioned for 100, and the contents of Sb, Dy, and Ti were relative to the percentage content of Sn element.

The theoretical value was each element's relative content of values, and the actual value was the electrode's EDS relative content value of the measured results. The results where the actual contents of electrode surface elements are compared with the theoretical values are given in Table 2.

From Table 2, the actual contents of Sb and Dy were lesser than the relative content of the theory, respectively, which might be related to the uniformity and stability of the sol. Various metal elements coexisting made coagulation easy, which could change the content of an element in sol. Not detecting the Ti element, explained that the surface of the coating was more uniform, and coating thickness was deeper than the monitoring depth of EDS.

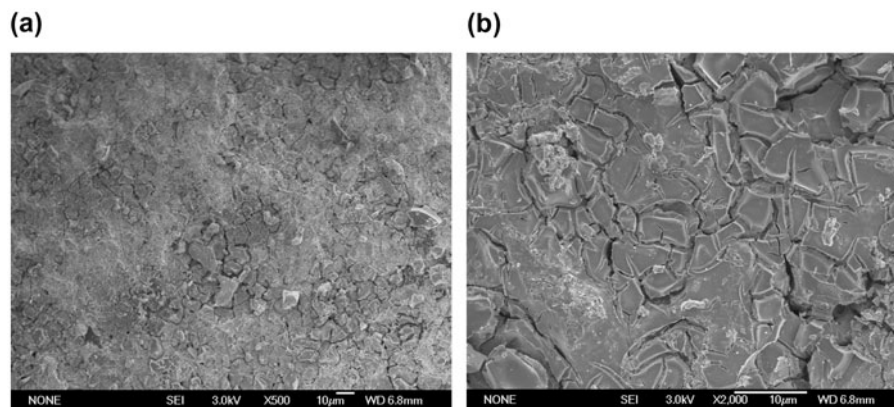


Fig. 2. Representative SEM images of the modified electrode surface layer (a) 500X and (b) 2000X.

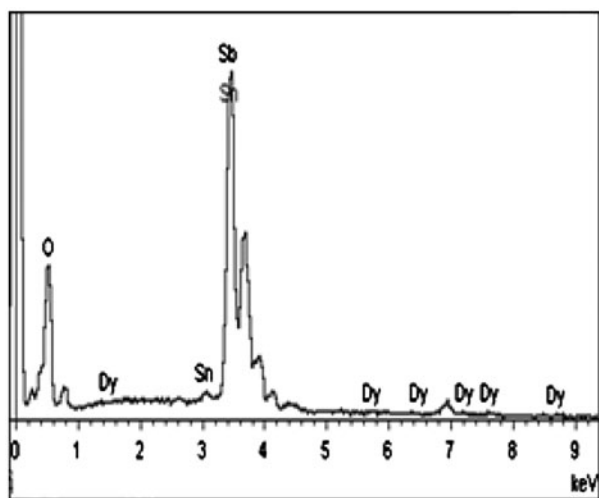


Fig. 3. EDS spectra of double coating Pr, Dy-doped Ti/SnO₂-Sb electrode.

The structural analysis was confirmed by a D/max-rA XRD instrument (Rigaku, Japan, Cu K α , 40 kV, 50 mA). From Fig. 4, it could be determined that the surface layer of the modified electrode had the tetragonal rutile-type structure of SnO₂ and formed solid solutions. From the XRD spectrum diagram, there were no Pr, Dy, or Sb corresponding oxide phases, and EDS testing result showed that there was a certain amount of doping elements, which suggested that Pr,

Dy, and Sb might enter the SnO₂ lattice in the form of interstitial, replacement, or disperse in the middle of the SnO₂ particles in the form of small clusters. So, the prepared anode might be described as Ti/SnO₂-Sb-Pr/SnO₂-Sb-Dy. The TiO₂ existed in the XRD spectra due to the metallic substrate. The average grain size of the electrode's surface coating was calculated as 3.3260 nm.

An electrode with a good stability could effectively provide service life (SL) for several years under normal conditions. To reduce the test time, the electrode's stability was assessed using the accelerated life test. In this section, the electrode plates' distance was reduced to 2 cm. The test was done at a constant anodic current density of 2×10^4 A cm⁻² in a 0.5 M H₂SO₄ electrolyte, and kept the cell temperature around 313 ± 1 K. The cell potential was monitored and the accelerated life was defined as the operation time at which the potential increased to above 10 V. Furthermore, a rough estimation for the electrode SL was derived from the method as Eq. (1), which was proposed by Hine and co-workers [38].

$$SL \sim 1/i^n \quad (1)$$

where i is the operating current density. N varies from 1.4 to 2.0, the average of which is assumed at 1.7 for the electrode [39].

Cyclic voltammetry measurement was carried out in the 0.5 M Na₂SO₄ solution with 25 mg L⁻¹ NIT, and

Table 2

Percentage of the electrode surface atom content of the table

Double coating Pr, Dy-doped Ti/SnO ₂ -Sb electrode	Sn	Sb/atomic%		Dy/atomic%		Ti/atomic%
		Theoretical	Observed	Theoretical	Observed	Observed
New	100	5	3.45	1.12	0.65	0

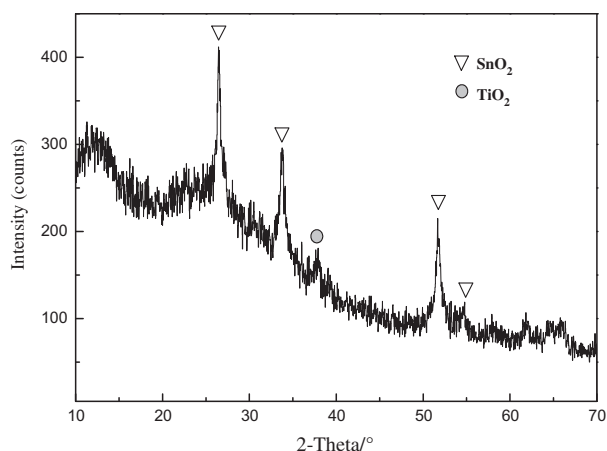


Fig. 4. XRD pattern of the surface layer of the modified electrode.

room temperature with a conventional three-electrode cell using the above-mentioned electrochemical workstation at a scan rate of 50 mV s^{-1} . The working electrode was the self-made Ti/SnO₂-Sb-Pr/SnO₂-Sb-Dy anode. A pure Ti plate was the counter electrode [40,41] and the reference was KCl saturated Hg/Hg₂Cl₂.

3. Results and discussion

3.1. The influence of the current density

The experiment that investigated the influence of current density on removal rate of NIT was carried out in the 0.3 M Na₂SO₄ solution with 25 mg L⁻¹ NIT at room temperature. There was a space (3 cm) between these two electrode plates cooperating magnetic stir.

Fig. 5 showed that with the increase in of the current density, the removal rate was on the rise. When the current density increased from 5 to 20 mA/cm², the removal rate increased from 48.5 to 48.5% after electrolysis 60 min. When the current density increased to 20 mA/cm², the removal rate had reached 100%, but slot voltage and electrolyte temperature were higher than the 10 mA/cm². When the current density is 10 mA/cm², the slot voltage and the electrolyte temperature were 5.2 V and 300 K, respectively. When the current density is 20 mA/cm², the slot voltage and the electrolyte temperature were 6.5 V and 307 K, respectively.

When the current density was lower, electron transfer rate and electrode reaction speed were slower, which made the speed of NIT removal slower. Increasing current density that meant the increase in

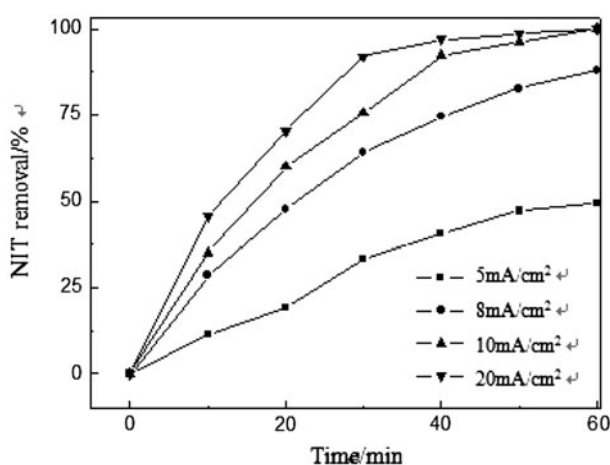


Fig. 5. The influence of the current density for removal rate of NIT.

the electron transfer rate and electrode reaction speed had an advantage in the removing speed of NIT. Nevertheless, the increase in current density also meant that oxygen evolution, hydrogen evolution, and other side effects were rising, and at the same time the heat generated by the electrolytic was also increasing, which resulted in increasing heat loss and decreasing current efficiency. All of them affected the treatment effect of the NIT. Considering these factors such as energy consumption and removal efficiency, 10 mA/cm² of current density was chosen.

3.2. Electrode stability and cyclic voltammetry

Good stability is a crucial parameter, which effects the application of an electrode. As stated above, an accelerated life test was performed for the fresh electrode to evaluate electrode stability. The results showed that Ti/SnO₂-Sb-Pr/SnO₂-Sb-Dy electrode was stable for about 54.6 h under accelerated conditions. Moreover, the real lifetime would be much longer and be affected by the test conditions, including pH, temperature of the electrolyte, and the current density. According to Eq. (1), the SL of the laboratory-prepared electrode in an application under 0.1 A cm⁻² current density and acidic electrolyte were predicted to be approximately 1.0 years. Fig. 6 presenting the maximum change percentage of the electrode potential in this test was 1.21% after 5 h. Thus, such an anode would keep a good performance on wastewater treatment with a long SL.

CV was performed to evaluate the electrode potential and the preliminary catalytic mechanism of NIT on the Ti/SnO₂-Sb-Pr/SnO₂-Sb-Dy electrode

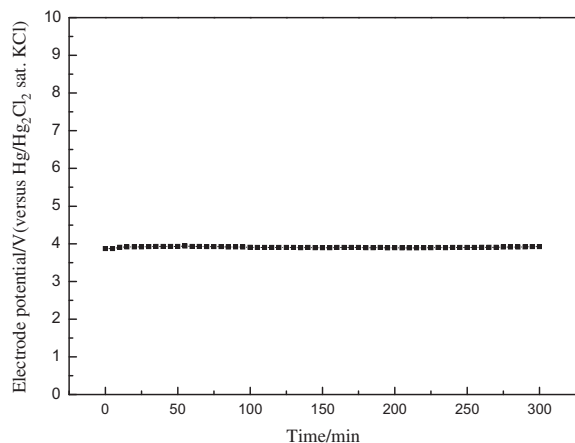


Fig. 6. The variation of the electrode potential in a 0.5 M H_2SO_4 electrolyte with the current density of $2 \times 10^4 \text{ A cm}^{-2}$, the electrode plate distance of 20 mm, the electrolysis area of 5.4 cm^2 , and $T = 313 \pm 1 \text{ K}$.

surface. According to Fig. 7, the oxygen evolution potential of the modified electrode was about 1.85 V (vs. $\text{Hg}/\text{Hg}_2\text{Cl}_2$), higher than the reported blank $\text{Ti}/\text{SnO}_2\text{-Sb}$ electrode (vs. $\text{Hg}/\text{Hg}_2\text{Cl}_2$) [42]. This outcome was desirable, because it is believed that the higher the oxygen evolution potential, the less unwanted power loss [43,44]. Meanwhile, electrodes before the oxygen evolution reaction did not have REDOX peak in the two kinds of solution. Adding NIT did not have an obvious effect on electrode cycle volt-ampere curve. These suggested that “direct electron-oxidation” [22,24,45] does not occur in the NIT degradation on the $\text{Ti}/\text{SnO}_2\text{-Sb-Pr}/\text{SnO}_2\text{-Sb-Dy}$

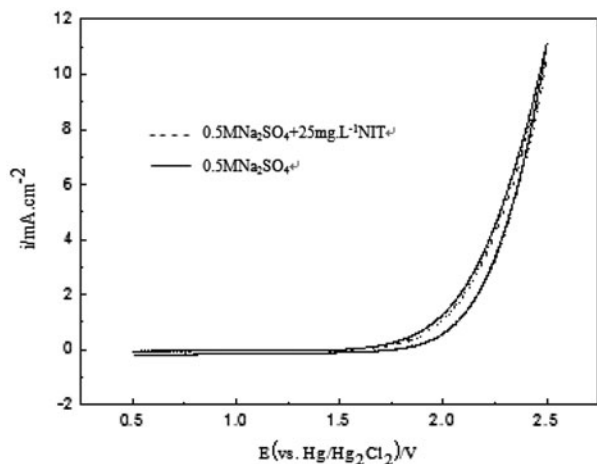


Fig. 7. Cyclic voltammograms of the $\text{Ti}/\text{SnO}_2\text{-Sb-Pr}/\text{SnO}_2\text{-Sb-Dy}$ anode obtained at a scan rate of 50 mV s^{-1} at the room temperature.

electrode. So “indirect electron-oxidation” [22,24,45,46] must be critical. Cui et al. [34] observed similar behavior for the oxidation of phenol on $\text{Ti}/\text{SnO}_2\text{-Sb-Re}$ (Re stands for the rare earth) electrode.

3.3. Kinetic study of NIT EC treatment

As stated above, our EC system was just involved in the indirect electron-oxidation of organics. The process is generally believed to take place in the first reaction for the formation of adsorbed oxygen radicals, especially hydroxyl radicals, which can be expressed by Eq. (2) [47,48].



Due to the adsorbing $\text{HO}_{\text{ads}}^{\cdot}$ on the anode, the initial chemical reaction between the radicals and NIT, can only occur when NIT transports from the solution towards the anode surface, i.e.



Meanwhile, the parallel reaction is the electrolysis of water molecules, i.e.



According to Eq. (3), the oxidation rate r for NIT molecules' EC degradation would be described as the following. Considering the concentration of its constant under the galvanostatic electrolysis:

$$r = \frac{d[\text{NIT}]}{dt} = k_{\text{NIT}}[\text{HO}^{\cdot}]^{\alpha}(\text{NIT})^{\beta} = k_{\text{app}(\text{NIT})}(\text{NIT})^{\beta} \quad (5)$$

k_{NIT} is the real rate constant. $k_{\text{app}(\text{NIT})}$ is the apparent rate constant of the NIT oxidation. α and β are the reaction orders relating to HO^{\cdot} and NIT molecules, respectively. Fig. 8 presents the variation of $\ln(\text{NIT}_0/\text{NIT}_t)$ (NIT_0 initial and NIT_t actual NIT concentration) as a function of its initial concentration. The straight lines obtained in these plots indicate that the kinetic of NIT EC degradation is in accordance with a pseudo-first-order reaction kinetics. The result is similar with the other organic pollutants oxidized on the anode [49]. Thus, Eq. (5) could be rewritten as Eqs. (6) and (7)

$$r = \frac{d[\text{NIT}]}{dt} = k_{\text{app}(\text{NIT})}(\text{NIT}) \quad (6)$$

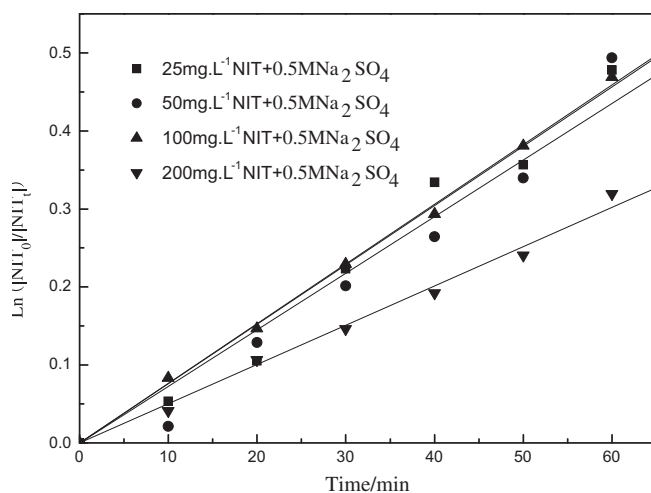


Fig. 8. Linear regression for the disappearance of NIT as a function of time via the Ti/SnO₂-Sb-Pr/SnO₂-Sb-Dy anode electrolysis at the room temperature with the current density of 10 mA cm⁻².

$$\ln \frac{(\text{NIT})_0}{(\text{NIT})_t} = k_{\text{app}(\text{NIT})} t = k_m \frac{S}{V} t \quad (7)$$

k_m stands for the apparent mass transfer coefficient. S is the electrolysis area, and V is the volume of the electrolyte.

Fig. 9 showed the removal amount of NIT for all cases after 60 min electrolysis and Table 3 summarized the relevant kinetic parameters for different initial NIT concentrations. In Fig. 9, it was obvious to observe that the higher the initial concentration of NIT, the

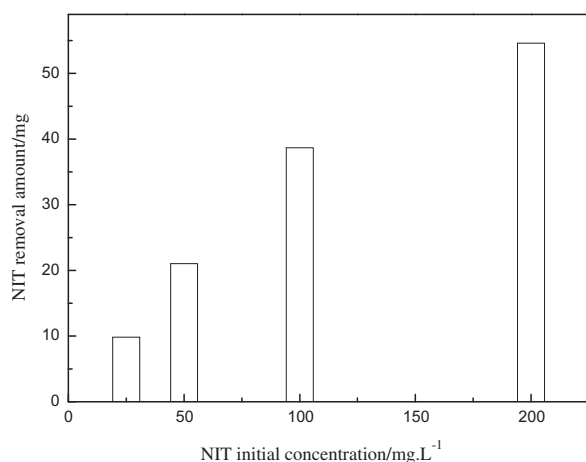


Fig. 9. The NIT removal amount as a function of NIT initial concentration via the Ti/SnO₂-Sb-Pr/SnO₂-Sb-Dy anode electrolysis at the room temperature with the current density of 10 mA cm⁻².

more is the NIT removal amount. This indicated that the mass transport had a significant effect on the NIT degradation. Table 3 also presented the increase of the mass transport rate ($k_{m(\text{NIT})}$) with the variation of NIT's initial concentration. However, interesting results were also found from Table 3. It could be seen that there were no significant differences at the apparent mass transfer coefficients (k_m) from 25 to 100 mg/L. But it obviously decreased at later stages (100–200 mg/L). It seemed that the oxidation of NIT was not only controlled by the rate ($k_{m(\text{NIT})}$) at which NIT molecules were carried from the solution to the anode surface. The chemical reaction (Eq. (3)) was another considerably influencing factor. Its influence could be explained by the competition from intermediates (the existing of intermediates was proven below), because HO[•] is a non-selective reactivity. A higher surface concentration of intermediates was produced as the NIT concentration increased. Moreover, the formation rate of oxygen (Eq. (4)) reduced in relation to the increasing NIT concentration process. This resulted in the subduction of the ability of gas stirring and brought about a decrease in the apparent mass transport.

3.4. Performance of the electrode on NIT degradation

Fig. 10 showed the efficiency of NIT and TOC abatement varying with time during galvanostatic electrolysis of NIT synthetic wastewater (100 mg/L). As it could be observed, after 180 min electrolysis, both parameters (NIT and TOC) were satisfactorily reduced, which indicated that the Ti/SnO₂-Sb-Pr/SnO₂-Sb-Dy-coated electrode is effective for NIT mineralization. Additionally, the rate of TOC removal began to increase later during the EC process. As a result, the overall rate of TOC removal was not a first-order over time, which suggested that there was formation and accumulation of different organic intermediates during NIT oxidation that were subsequently degraded at different rates by the electrodes. Other authors also reported similar behavior in the anode electrolysis of refractory wastewaters [33,50].

The variations of the NIT wastewater samples' UV absorption spectrum from 190 to 400 nm were illustrated in Fig. 11 within 180 min electrolysis time. It was observed that there were two maximum absorption spectra, which were 220 and 270 nm. At the end of electrolysis (180 min), the spectrum was obviously different: a band with a maximum at 270 nm almost disappeared and a broader absorption band covering the wavelength range 220–245 nm could be observed. The change in the spectrum during the NIT EC

Table 3

$k_{app(NIT)}$ (apparent rate constants), $k_{m(NIT)}$ (mass transport rate), and k_m (apparent mass transfer coefficient) of NIT as a function of initial NIT concentration via the Ti/SnO₂-Sb-Pr/SnO₂-Sb-Dy anode 60 min electrolysis

Initial concentration of NIT (mg L ⁻¹)	25	50	100	200
$k_{app(NIT)}$ (h ⁻¹)	0.00761	0.00725	0.00765	0.00503
$k_{m(NIT)}$ (mg m ⁻² s ⁻¹)	5.06	10.81	19.90	28.09
k_m (10 ⁻⁷ m s ⁻¹)	5.87	5.59	5.90	3.88

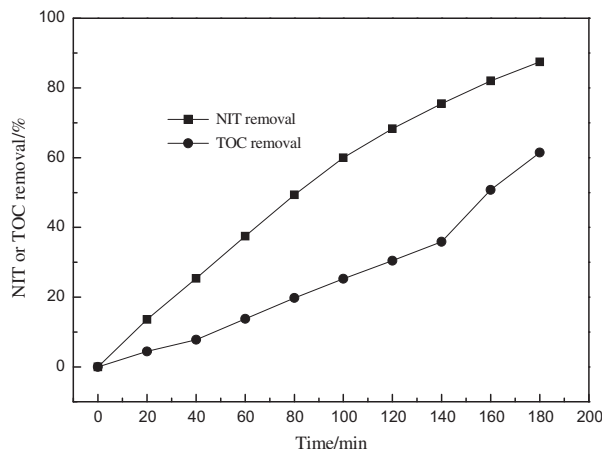


Fig. 10. Variation of NIT and TOC removal for 100 mg L⁻¹ NIT during the electrolysis time of 0–180 min with the Ti/SnO₂-Sb-Pr/SnO₂-Sb-Dy anode and the current density of 10 mA cm⁻² at the room temperature.

degradation might be ascribed to pyridine-containing intermediates.

3.5. Degradation pathway and mechanism analyses

Based on the above analyses and the main molecular ion fragmentation peaks, Table 4 summarized the EIS-Q-TOF-MS qualitative analysis of NIT-relating stable degradation products. A degradation pathway involving these detected products was proposed for the EC mineralization of NIT in neutral media as shown in Fig. 12. Some undetected compounds were also written out in the brackets of Fig. 12 in terms of the molecular fragmentation patterns. These compounds could readily and rapidly be oxidized or hydrolyzed to small inorganic molecules.

HO[•] specie, an electrophilic radical, is an oxidizing reagent with high efficiency and favors to attack the positions with a big density for electron cloud in organic molecules. As Fig. 12 showed, the EC oxidative degradation of the NIT at the Ti/SnO₂-Sb-Pr/SnO₂-Sb-Dy anode began with the reaction between

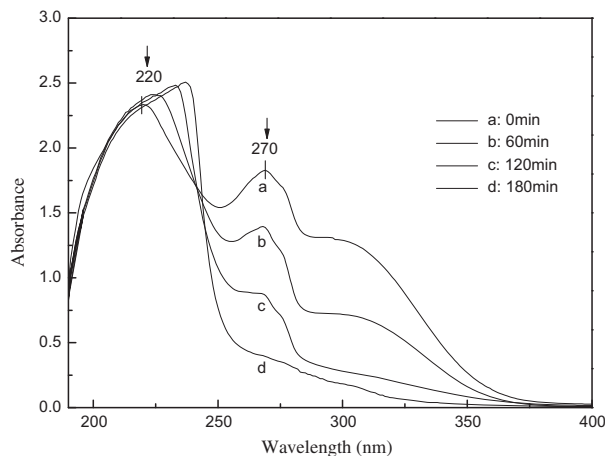
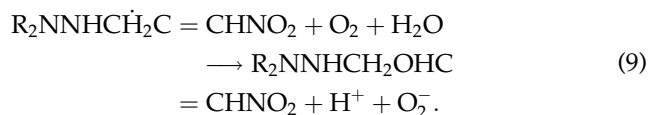
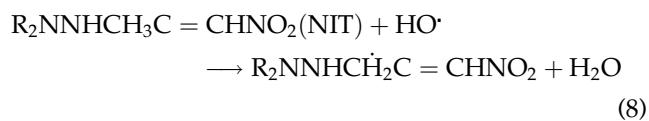


Fig. 11. UV absorption spectrum of the electric degradation of NIT during the electrolysis time of 0–180 min.

the HO[•] group and the α -C of imino N to yield (E)-N-[(6-chloropyridin-3-yl)methyl]-N-ethyl-2-nitroethene-1,1-diamine (compound 1). The mechanism involved H-abstraction to produce water and α -amino radical ($R_2NNHCH_2C = \dot{C}HNO_2$) (Eq. (8)). The latter radical had a reduction property [51]. Hence, it might further react with dissolved dioxygen to generate superoxide radical ($O_2^{\cdot-}$) and hydroxyethylamine after adding water (Eq. (9)). Hydrolysis of hydroxyethylamine led to the formation of compound 1 and formaldehyde as shown in Fig. 10.

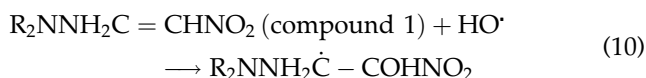


The initial degradation step was similar with the primary photolysis oxidation of acetamiprid reported

Table 4
EIS-QTOF-MS data for NIT and several stable degradation intermediate products

Symbol	Proposed product		Calculated <i>m/z</i> value	Observed <i>m/z</i> value	MS deviation
	Molecular formula	Compound name			
Parent substance	C ₁₁ H ₁₅ ClN ₄ O ₂	(E)-N-[(6-chloropyridin-3-yl)methyl]-N-ethyl-N-methyl-2-nitroethene-1,1-diamine	270.0884	271.0939	-1.0055
1	C ₁₀ H ₁₃ ClN ₄ O ₂	(E)-N-[(6-chloropyridin-3-yl)methyl]-N-ethyl-2-nitroethene-1,1-diamine	256.0727	256.0892	-0.0165
2	C ₁₀ H ₁₄ ClN ₃ O	(Z)-2-amino-2-[(6-chloropyridin-3-yl)methyl](ethyl)amino} ethanol	227.0825	227.0342	-0.0483
3	C ₁₀ H ₁₃ ClN ₂ O	2-[(6-chloropyridin-3-yl)methyl](ethyl)amino} acetaldehyde	212.0716	212.0948	-0.0232
4	C ₁₀ H ₁₄ N ₂ O	2-[ethyl(pyridin-3-ylmethyl)amino]acetaldehyde	178.1106	178.1334	-0.0228
5	C ₁₀ H ₁₄ N ₂ O ₂	2-[ethyl[(6-hydroxypyridin-3-yl)methyl]amino} acetaldehyde	194.1055	193.0714	+1.0341
6	C ₈ H ₁₃ NO ₂	(E)-4-[ethyl(2-oxoethyl)amino]but-2-enal	155.0946	155.0811	+0.0135
7	C ₆ H ₅ NO ₄	2-[ethyl(2-hydroxyethyl)amino]acetaldehyde	131.0946	131.0802	+0.0144

by Maria et al. [9]. Compound 1 was then further transformed to (Z)-2-amino-2-[(6-chloropyridin-3-yl)methyl](ethyl)amino} ethanol (compound 2) in the HO[•]-mediated system. Since compound 2 contained an olefinic alcohol structure, it could undergo structural rearrangement to form the aldehyde derivative of 2-amino-2-[(6-chloropyridin-3-yl)methyl](ethyl)amino} acetaldehyde with better stability. In the conversion of compound 1 to compound 2, the HO[•] radical first attacked the C=C bond of the side chain by adding it to the π system (Eq. (10)), and then substituting -NO₂ (an electron-withdrawing group) detached from the C=C moiety after seizing an electron from the novel producing organic radical as shown in Eq. (10). The addition of hydroxyl radical to the π system associated with the detachment of other strong electron-withdrawing, which was substituted by the same carbon atom, has been reported numerous times [39,52,53].



Subsequent attacking of hydroxyl radicals at the in situ generated amino group of the side chain after the first oxidation step (NIT \rightarrow compound 1) involves deamination redox reaction due to its high electron donor capacity. This reaction led to the formation of 2-[(6-chloropyridin-3-yl)methyl](ethyl)amino} acetaldehyde (compound 3) and hydroxylamine. The succeeding product of the anterior intermediate was 2-[ethyl(pyridin-3-ylmethyl)amino]acetaldehyde (compound 4), the existence of which suggested a

dechlorination process on the pyridine ring. Although, Cl⁻ is a strong electron-withdrawing substituent of the pyridine ring, this process did not involve a favorable electrophilic addition of hydroxyl radical with the relevant carbon atom of the π system as stated above. On the other hand, the most prominent peak, meaning the biggest relative intensity in the MS spectrum after 120 min of electrolysis, was identified for compound 3. This fact supports that compound 3 could not be attacked easily by HO[•]. Therefore, under our conditions, the conversion of compound 3 to compound 4 might attribute to another in situ generating oxidant, H₂O₂ (see Fig. 13). In anode EC theories, the production of H₂O₂ is proposed through the reduction reaction of O₂ in the cathode as follows:



There are principally two kinds of electrode materials: the so-called "active" and "non-active" anodes. The active anodes, such as Pt, IrO₂, and RuO₂-based coatings, could do the reaction of Eq. (11) to produce H₂O₂ finally [33,47,50,54]. However, the non-active anodes, like PbO₂- and SnO₂-Sb-based series, do not involve the direct electron transfer of Eq. (11) to generate and produce H₂O₂ [33,39]. Therefore, the detected H₂O₂ must come from another process, in which the formation of H₂O₂ was due to the reduction property

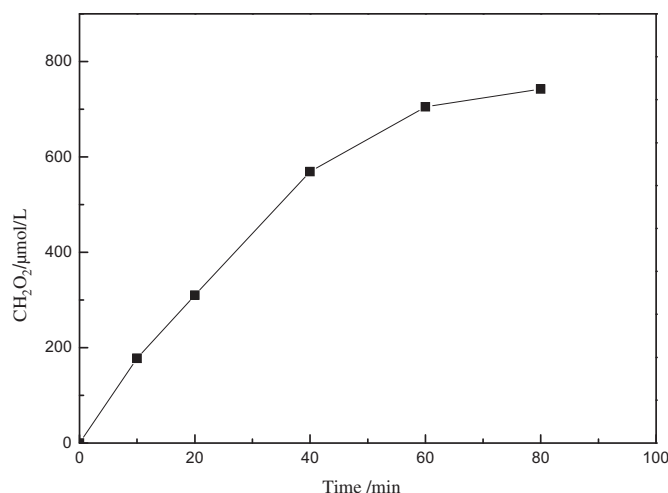
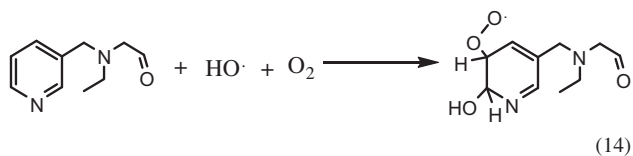


Fig. 13. Variation of the concentration of in situ-generated H₂O₂ during the EC degradation of NIT.

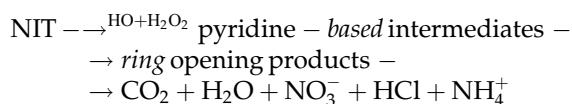
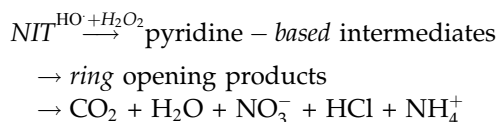
is faster than its consumption rate for the conversion of compound 3 to compound 4.

After the chlorine atom leaving the pyridine ring, compound 4 seemed to be reactive towards HO[•]. A second electrophilic addition of hydroxyl radical with the pyridine ring provoked the formation of peroxy radical (Eq. (14)), leading to the conversion of compound 4 to hydroxypyridine compound of 2-[ethyl [(6-hydroxypyridin-3-yl) methyl] amino] acetaldehyde (compound 5) after releasing . The similitude process also could be found in the conversion of 2, 4-DCR to its dehydroxylation derivative, 4, 6-DCR [52]. In this degradation pathway (Fig. 12), the next reaction step of the pyridine ring cleavage was proposed. Products obtained from the C–C bonds of pyridine ring breaking were identified with (E)-4-[ethyl (2-oxoethyl) amino] but -2-enal (compound 6) and iminodicarbonic acid. Compound 6 could be further oxidized to 2-[ethyl (2-hydroxyethyl) amino] acetaldehyde (compound 7) to ethyliminodicarbonic acid. Under oxidizing conditions, ethyliminodicarbonic acid was finally mineralized to CO₂, H₂O, and NH₄⁺.



As observed for NIT, intermediates were mainly composed of pyridine derivatives (compounds 1–5) as indicated by UV absorption spectrum analysis. The evidences of product identification displayed that the pyridine moiety could be attacked for the ring

rejection to take place by combining of oxidizing agents like H₂O₂ with EC organic oxidation. Thus, the mineralization reaction of NIT could be summarized as follows:



3.6. Energy consumption estimation

The energy consumption per volume of treated effluent was estimated and expressed in kWh m⁻³. The average cell voltage, during the electrolysis, was taken for calculating the energy consumption, as follows:

$$\text{Energy consumption} = \left(\frac{V \times A \times t}{1000 \times V_s} \right) \quad (15)$$

where t is the time of electrolysis (h); V and A are the average cell voltage and the electrolysis current, respectively; and V_s is the sample volume (m³).

Table 5 presented the energy consumption required per volume of treated effluent at a different applied current density. As it could be observed, during the electrolyses of NIT synthetic wastewaters, the energy consumption seemed to be proportional to the applied current density. For example, it increased

Table 5

Energy consumption calculated from Eq. (15), per volume of treated effluent during anodic oxidation of NIT for: different applied current densities $[\text{NIT}]_0 = 25 \text{ mgL}^{-1}$, electrolyte: $0.3\text{M Na}_2\text{SO}_4$

Applied current density (mA cm^{-2})	Energy consumption (kWh m^{-3})	Electrical energy cost
5	5.31	2.947
8	5.60	3.108
10	7.95	4.412
20	11.43	6.344

from 5.31 to 11.43 kWh m^{-3} of effluent treated when the current density passed from 5 to 20 mA cm^{-2} [50].

Finally, taking into consideration an electrical energy cost of about $\text{¥}0.555$ (The price of Shan dong province) per kWh, the process expenditure was estimated and reported in Table 5.

$$\text{Cost} (\text{¥m}^{-3}) = \text{Energy consumption} (\text{kWh m}^{-3}) \times 0.3 (\text{¥kWh}) \quad (16)$$

4. Conclusion

The $\text{Ti/SnO}_2\text{-Sb-Pr/SnO}_2\text{-Sb-Dy}$ anode showed a nice electro-catalysis performance for the degradation of NIT. The removal efficiency of NIT and TOC reached 87.45 and 61.46% after 180 min electrolysis for synthetic wastewater containing 100 mg/L NIT and $0.5 \text{ M Na}_2\text{SO}_4$ supporting electrolyte, respectively, when operating at the current density of 10 mA cm^{-2} . The kinetic of NIT EC degradation was in accordance with a pseudo-first-order reaction kinetics. Based on the experimental analyses, a mineralization pathway was proposed for NIT in neutral media. 2-[(6-chloropyridin-3-yl) methyl] (ethyl)amino)acetaldehyde was identified as the main intermediate product before the pyridine ring cleavage, which took place after hydroxylation of the ring, ultimately leading to the transformation of NIT to ring-opening products to small inorganic molecules. The mineralization mechanism involved the attack of HO^\bullet and H_2O_2 . The latter active material was produced from the reaction between dioxygen and α -amino radical, which in situ generated during the EC oxidation of NIT. Hereby, the formation of H_2O_2 was limited by the concentration of dissolved oxygen in aqueous solution. In order to improve the removal efficiency of the method, increase of aeration system to EC treatment process seemed a suitable means.

Considering the combining of such EC process with biological treatment technology might be another feasible and economical alternative for the NIT treatment. When no pyridine-containing products

remained, the electrolysis could be stopped. The remaining ring-opening products were biodegradable. Thus, subsequent biological process could finish the complete mineralization. In general, such advanced EC oxidation technique appeared to be an attractive alternative for pre-treatment or treatment of recalcitrant toxic wastewater containing NIT or other neonicotinoid insecticides.

Acknowledgements

The research was supported by the Technological Progress Plan of Shandong, grant no. 2011GGE27048, China.

Abbreviations

NIT	—	nitenpyram
EC	—	electro-catalytic
ESI-Q-TOF-MS	—	electrospray ionization quadrupole time-of-flight tandem mass spectrometry
SL	—	the service life

References

- [1] P. Jeschke, R. Nauen, M. Schindler, A. Elbert, Overview of the status and global strategy for neonicotinoids, *J. Agric. Food. Chem.* 59 (2011) 2897–2908.
- [2] P. Jeschke, R. Nauen, Neonicotinoids-from zero to hero in insecticide chemistry, *Pest Manage. Sci.* 64 (2008) 1084–1098.
- [3] P.N. Moza, K. Hustert, E. Feicht, A. Kettrup, Photolysis of imidacloprid in aqueous solution, *Chemosphere* 36 (1998) 497–502.
- [4] S. Malato, J. Blanco, A. Vidal, D. Alarcón, M.I. Maldonado, J. Cáceres, W. Gernjak, Applied studies in solar photocatalytic detoxification: An overview, *Sol. Energ.* 75 (2003) 329–336.
- [5] S. Malato, J. Blanco, J. Cáceres, A.R. Fernández-Alba, A. Agüera, A. Rodríguez, Photocatalytic treatment of water-soluble pesticides by photo-Fenton and TiO_2 using solar energy, *Catal. Today* 76 (2002) 209–220.

- [6] S. Malato, J. Caceres, A. Agüera, M. Mezcua, D. Hernando, J. Vial, A.R. Fernández-Alba, Degradation of imidacloprid in water by photo-fenton and TiO₂ photocatalysis at a solar pilot plant: A comparative study, *Environ. Sci. Technol.* 35 (2001) 4359–4366.
- [7] G. Mailhot, M. Sarakha, B. Lavedrine, J. Cáceres, S. Malato, Fe(III)-solar light induced degradation of diethyl phthalate (DEP) in aqueous solutions, *Chemosphere* 49 (2002) 525–532.
- [8] V.J. Guzsvány, J.J. Csanádi, S.D. Lazić, F.F. Gaál, Photocatalytic degradation of the insecticide acetamiprid on TiO₂ Catalyst, *J. Braz. Chem. Soc.* 20 (2009) 152–159.
- [9] M.L. Dell’Arciprete, L. Santos-Juanes, A.A. Sanz, R. Vicente, A.M. Amat, J.P. Furlong, D.O. Mártire, M.C. Gonzalez, Reactivity of hydroxyl radicals with neonicotinoid insecticides: Mechanism and changes in toxicity, *Photochem. Photobiol. Sci.* 8 (2009) 1016–1023.
- [10] V. Kitsiou, N. Filippidis, D. Mantzavinos, I. Poulis, Heterogeneous and homogeneous photocatalytic degradation of the insecticide imidacloprid in aqueous solutions, *Appl. Catal. B. Environ.* 86 (2009) 27–35.
- [11] U. Černigoj, U.L. Štangar, P. Trebše, Degradation of neonicotinoid insecticides by different advanced oxidation processes and studying the effect of ozone on TiO₂ photocatalysis, *Appl. Catal. B. Environ.* 75 (2007) 229–238.
- [12] A. Elbert, M. Haas, B. Springer, W. Thielert, R. Nauen, Applied aspects of neonicotinoid uses in crop protection, *Pest Manage. Sci.* 64 (2008) 1099–1105.
- [13] I. Yamamoto, J.E. Casida, *Nicotinoid Insecticides and the Nicotinic Acetylcholine Receptor*, Springer-Verlag, Tokyo, 1999.
- [14] Y. Tsumura, Y. Nakamura, Y. Tonogai, Y. Kakimoto, Y. Tanaka, T. Shibata, Determination of neonicotinoid pesticide nitenpyram and its metabolites in agricultural products, *J. Food. Hyg. Soc. Jpn.* 39 (1998) 127–134.
- [15] C.Q. Zhang, J. Hu, M.H. Wang, Hydrolysis and photolysis behavior of nitenpyram, *Ecol. Environ. Sci.* 20 (2011) 1735–1738.
- [16] Y.J. Feng, X.Y. Li, Electro-catalytic oxidation of phenol on several metal-oxide electrodes in aqueous solution, *Water Res.* 37 (2003) 2399–2407.
- [17] S.P. Li, H.B. Wang, J.F. Lian, X.Y. Zeng, Preparation and characterization of Nd-doped Ti/SnO₂-Sb₂O₅ electro-catalytic electrodes used for reactive brilliant red X-3B wastewater treatment, *Adv. Mater. Res.* 455 (2012) 1356–1360.
- [18] A.M. Polcaro, S. Palmas, F. Renoldi, M. Mascia, On the performance of Ti/SnO₂ and Ti/PbO₂ anodes in electrochemical degradation of 2-chlorophenol for wastewater treatment, *J. Appl. Electrochem.* 29 (1999) 147–151.
- [19] E. Brillas, J.C. Calpe, J. Casado, Mineralization of 2,4-D by advanced electrochemical oxidation processes, *Water Res.* 34 (2000) 2253–2262.
- [20] E. Brillas, I. Sirés, M.A. Oturan, Electro-Fenton process and related electrochemical technologies based on Fenton’s reaction chemistry, *Chem. Rev.* 109 (2009) 6570–6631.
- [21] C.A. Martínez-Huitle, E. Brillas, Decontamination of wastewaters containing synthetic organic dyes by electrochemical methods: A general review, *Appl. Catal. B. Environ.* 87 (2009) 105–145.
- [22] C.A. Martínez-Huitle, E. Brillas, Electrochemical alternatives for drinking water disinfection, *Angew. Chem. Int. Ed.* 47 (2008) 1998–2005.
- [23] M. Panizza, G. Cerisola, Direct and mediated anodic oxidation of organic pollutants, *Chem. Rev.* 109 (2009) 6541–6569.
- [24] G.H. Chen, Electrochemical technologies in wastewater treatment, *Sep. Purif. Technol.* 38 (2004) 11–41.
- [25] Z.X. Zhang, Forty-year development of titanium-anode, *Chlor-Alkali. Ind.* 1008-133X (2007) 01–0015.
- [26] B.O. Park, C.D. Lokhande, H.S. Park, K.D. Jung, O.S. Joo, Cathodic electrodeposition of RuO₂ thin films from Ru(III)Cl₃ solution, *Mater. Chem. Phys.* 87 (2004) 59–66.
- [27] C.P. De Pauli, S. Trasatti, Composite materials for electrocatalysis of O₂ evolution: IrO₂+SnO₂ in acid solution, *J. Electroanal. Chem.* 538–539 (2002) 145–151.
- [28] J.M. Hu, J.Q. Zhang, C.N. Cao, Oxygen evolution reaction on IrO₂-based DSA type electrodes: Kinetics analysis of Tafel lines and EIS, *Int. J. Hyd. Eng.* 29 (2004) 791–797.
- [29] V. Sáez, J. González-García, J. Iniesta, Electrodeposition of PbO₂ glassy carbon electrodes: Influence of ultrasound frequency, *Electrochem. Commun.* 4 (2002) 370–373.
- [30] Y.J. Feng, Y.L. Xiao, Electrochemical degradation of phenol: Performance of several metal oxides-based anodes, *Water. Res.* 37 (2003) 1099–1103.
- [31] X.Y. Li, Y.H. Cui, Y.J. Feng, Z.M. Xie, J.D. Gu, Reaction pathways and mechanisms of the electrochemical degradation of phenol on different electrodes, *Water Res.* 39 (2005) 1972–1981.
- [32] Y.J. Feng, Y.H. Cui, Factors affecting the electro-catalytic characteristics of Eu doped SnO₂/Sb electrode, *J. Hazard. Mater.* 178 (2010) 29–34.
- [33] Y.J. Feng, Y.H. Cui, B. Logan, Z.Q. Liu, Performance of Gd-doped Ti-based Sb-SnO₂ anodes for electrochemical destruction of phenol, *Chemosphere* 70 (2008) 1629–1636.
- [34] H. Obana, M. Okihashi, K. Akutsu, Y. Kitagawa, S. Hori, Determination of acetamiprid, imidacloprid, and nitenpyram residues in vegetables and fruits by high-performance liquid chromatography with diode-array detection, *J. Agric. Food. Chem.* 50 (2002) 4464–4467.
- [35] J. Wang, D. Leung, Analyses of macrolide antibiotic residues in eggs, raw milk, and honey using both ultra-performance liquid chromatography/quadrupole time-of-flight mass spectrometry and high-performance liquid chromatography/tandem mass spectrometry, *Rapid. Commun. Mass. Spectrom.* 21 (2007) 3213–3222.
- [36] T.J.P. Smyth, V.R. Robledo, W.F. Smyth, Characterisation of oxazepam degradation products by high-performance liquid chromatography/electrospray ionisation mass spectrometry and electrospray ionization quadrupole time-of-flight tandem mass spectrometry, *Rapid. Commun. Mass. Spectrom.* 24 (2010) 651–658.
- [37] A.A. Joshi, B.R. Locke, P. Arce, W.C. Finney, Formation of hydroxyl radicals, hydrogen peroxide and aqueous electrons by pulsed streamer corona discharge in aqueous solution, *J. Hazard. Mater.* 41 (1995) 3–30.

- [38] F. Hine, M. Yasuda, T. Noda, T. Yoshida, J. Okuda, Electrochemical behavior of the oxide-coated metal anodes, *J. Electrochem. Soc.* 126 (1979) 1439–1445.
- [39] M.H. Zhou, Q.Z. Dai, L.C. Lei, C.A. Ma, D.H. Wang, Long life modified lead dioxide anode for organic wastewater treatment: Electrochemical characteristics and degradation mechanism, *Environ. Sci. Technol.* 39 (2005) 363–370.
- [40] X. Yang, R. Zou, F. Huo, D. Cai, D. Xiao, Preparation and characterization of Ti/SnO₂-Sb₂O₃-Nb₂O₅/PbO₂ thin film as electrode material for the degradation of phenol, *J. Hazard. Mater.* 164 (2009) 367–373.
- [41] J. Iniesta, J. González-García, E. Expósito, V. Montiel, A. Aldaz, Influence of chloride ion on electrochemical degradation of phenol in alkaline medium using bismuth doped and pure PbO₂ anodes, *Water Res.* 35 (2001) 3291–3300.
- [42] S.P. Li, J.F. Lian, H.B. Wang, Dye wastewater treatment using self-made Nd doped Ti/SnO₂-Sb electro-catalytic electrodes, *Asian. J. Chem.* 6 (2011) 2491–2496.
- [43] R. Kötzt, S. Stucki, B. Carcer, Electrochemical waste water treatment using high overvoltage anodes. Part I: Physical and electrochemical properties of SnO₂ anodes, *J. Appl. Electrochem.* 21 (1991) 14–20.
- [44] S. Stucki, R. Kötzt, B. Carcer, W. Suter, Electrochemical waste water treatment using high overvoltage anodes. Part II: Anode performance and applications, *J. Appl. Electrochem.* 21 (1991) 99–104.
- [45] J. Iniesta, P.A. Michaud, M. Panizza, G. Cerisola, A. Aldaz, C. Comninellis, Electrochemical oxidation of phenol at boron-doped diamond electrode, *Electrochim. Acta* 46 (2001) 3573–3578.
- [46] Y.H. Cui, Y.J. Feng, Z.Q. Liu, Influence of rare earths doping on the structure and electro-catalytic performance of Ti/Sb-SnO₂ electrodes, *Electrochim. Acta* 54 (2009) 4903–4909.
- [47] C. Comninellis, Electrocatalysis in the electrochemical conversion/combustion of organic pollutants for waste water treatment, *Electrochim. Acta* 39 (1994) 1857–1862.
- [48] O. Simond, V. Schaller, C. Comninellis, Theoretical model for the anodic oxidation of organics on metal oxide electrodes, *Electrochim. Acta* 42 (1997) 2009–2012.
- [49] Y. Samet, S.C. Elaoud, S. Ammar, R. Abdelhedi, Electrochemical degradation of 4-chloroguaiacol for wastewater treatment using PbO₂ anodes, *J. Hazard. Mater.* 138 (2006) 614–619.
- [50] G.R. de Oliveira, N.S. Fernandes, J.V.D. Melo, D.R. da Silva, C. Urgeghe, C.A. Martínez-Huitle, Electro-catalytic properties of Ti-supported Pt for decolorizing and removing dye from synthetic textile wastewaters, *Chem. Eng. J.* 168 (2011) 208–214.
- [51] K.O. Hiller, K.D. Asmus, Formation and reduction reactions of α -amino radicals derived from methionine and its derivatives in aqueous solutions, *J. Phys. Chem.* 87 (1983) 3682–3688.
- [52] M.A. Oturan, An ecologically effective water treatment technique using electrochemically generated hydroxyl radicals for *in situ* destruction of organic pollutants: Application to herbicide 2,4-D, *J. Appl. Electrochem.* 30 (2000) 475–482.
- [53] S. Song, L.Y. Zhan, Z.Q. He, L.L. Lin, J.J. Tu, Z.H. Zhang, J.M. Chen, L.J. Xu, Mechanism of the anodic oxidation of 4-chloro-3-methyl phenol in aqueous solution using Ti/SnO₂-Sb/PbO₂ electrodes, *J. Hazard. Mater.* 175 (2010) 614–621.
- [54] Y.Q. Wang, B. Gu, W.L. Xu, Electro-catalytic degradation of phenol on several metal-oxide anodes, *J. Hazard. Mater.* 162 (2009) 1159–1164.